A Multirate Approach for Fluid-Structure Interaction Computation with Decoupled Methods

Lian Zhang*, Mingchao Cai†, and Mo Mu‡

Abstract. We investigate a multirate time step approach applied to decoupled methods in fluid and structure interaction(FSI) computation, where two different time steps are employed for fluid and structure respectively. For illustration, the multirate technique is examined by applying the decoupled β scheme. Numerical experiments show that the proposed approach is stable and retains the same order of accuracy as the original single time step scheme, while with much less computational expense.

AMS subject classifications: 65M12, 37N10, 65N22, 65N30, 65M60, 65P99

Key words: Fluid and structure interaction (FSI), decoupled methods, multirate time step, stability, β scheme.

1 Introduction

Fluid structure interaction (FSI) finds many important applications in science and engineering [3–5, 7, 15–17, 25–27]. Numerical FSI methods may be generally classified as fully implicit and decoupled approaches. The fully implicit approach leads to coupled schemes [29], in which the equations of fluid dynamics, structural mechanics, and mesh moving are solved simultaneously in a fully coupled fashion. Although the coupled schemes are unconditionally stable in general, they usually result in significant difficulties and inflexibility in the design and choice of mesh generation, PDE discretization, algebraic solvers, as well as software development. On the other hand, certain decoupled approaches, often called loosely coupled, or partitioned, or explicit coupling approaches, have been investigated [1, 2, 13, 20], where the equations of fluid dynamics, structural mechanics, and mesh moving are solved locally so that existing fluid and structure solvers may be applied by easy software integration. There are many other important physical and numerical considerations that appeal to decoupled methods for treating different sub-models in their own physical regions independently, particularly

*E-mail address: lzhangay@connect.ust.hk. Department of Mathematics, the HongKong University of Science and Technology.

†Corresponding author. E-mail address: cmchao2005@gmail.com. Department of Mathematics, Morgan State University.

‡E-mail address: mamu@ust.hk. Department of Mathematics, the HongKong University of Science and Technology.

because the fluid and solid possess very different physical properties and time scales. This is generally true, not only for FSI problems [6, 11, 14–16, 27, 29], but also for other coupled multi-domain, multi-physics applications [8, 9, 18, 19, 21–24].

Due to different time scales in many multi-physics applications, it is natural and important to develop multirate time-stepping schemes that mimic the physical phenomena. A multirate time-step technique was introduced in [21, 22] for decoupled methods of coupled fluid-porous media flow models, where the entire time interval $[0, T]$ is first partitioned into certain coarse time-grids with the time-step size τ_{coarse}. Within each coarse-time grid, the free fluid flow solutions are computed for multiple fine-time steps with the boundary information at the interface from the porous medium solution at the beginning of the current coarse-time grid. When the computation reaches the end of current coarse-time grid, the porous medium solution is then updated by using the data from the fluid region. Such a multirate approach is proved to be stable. Other multi-domain, multi-physics applications which adopt multirate time-step technique can be found in [23, 24].

We propose to develop multirate decoupled algorithms for FSI applications in this paper. It has been observed that decoupled methods might lead to instability for certain FSI applications, such as the coupling of an incompressible Stokes flow with a thin-walled structure, due to the artificial added-mass effect if the coupled FSI model is not properly decoupled [10, 12]. It has become one of the major challenges recently to develop stable decoupled methods without added-mass effects for such applications. For the benchmark problem of the coupled incompressible Stokes flow with a thin-walled structure, two decoupled methods have been devised recently, one is the Robin-Neumann scheme [11] and the other is the so-called β scheme [6]. Both algorithms are shown to be stable without added-mass effects [6, 11].

Note that the structure variables vary much more rapidly than the fluid variables in this application. We thus propose to apply the multirate time-stepping to these stable decoupled schemes. For illustration, we will examine the application of the multirate technique to the β scheme, since similar performance is observed for both the Robin-Neumann scheme and the β scheme in numerical experiments. Numerical experiments demonstrate that the proposed approach is stable and retains the same order of accuracy as the original single time step schemes, while with much less computational expense. Furthermore, the decoupled multirate β scheme may be extended to more general FSI problems involving nonlinearity, irregular domains, and large structural deformations, which is illustrated by a computational biomechanical model for abdominal aneurysm simulation.

The paper is organized as follows. In Section 2, we describe the coupled model of a Stokes flow with a thin-walled structure. In Section 3, the multirate β scheme is presented for the coupled model. Numerical experiments are presented in Section 4 to show the stability, convergence, and efficiency of the multirate β scheme. Concluding remarks are given in Section 5.

2 A Benchmark Model of a Stokes Flow Interacting with a Thin-Walled Structure

We describe below the benchmark model of a stokes flow interacting with a thin-walled structure as studied in [6, 11], where the fluid motion is governed by the Stokes equations in a d-dimensional ($d=2,3$) domain Ω_f and the structure is assumed to be a linear thin-solid defined on a $(d-1)-$ manifold Γ. Denote $\partial\Omega_f=\Gamma\cup\Gamma_D\cup\Gamma_N$ to be the boundary of Ω_f, consisting of the fluid-structure interface Γ, as well as Γ_D and Γ_N for the fluid boundaries with Dirichlet and Neumann conditions imposed externally. The coupled model then reads as: finding the fluid velocity $\boldsymbol{u}_f:\Omega_f\times\mathbb{R}^+\to\mathbb{R}^d$, the fluid pressure $p_f:\Omega_f\times\mathbb{R}^+\to\mathbb{R}$, and the solid displacement $\boldsymbol{d}:\Gamma\times\mathbb{R}^+\to\mathbb{R}^{d-1}$ such that

$$\begin{cases} \rho_f\partial_t\boldsymbol{u}_f-\mathrm{div}\sigma_f(\boldsymbol{u}_f,p_f)=0 & \text{in} \quad \Omega_f,\\ \mathbf{div}\boldsymbol{u}_f=0 & \text{in} \quad \Omega_f,\\ \boldsymbol{u}_f=0 & \text{on} \quad \Gamma_D,\\ \sigma_f(\boldsymbol{u}_f,p_f)\boldsymbol{n}=\boldsymbol{f}_N & \text{on} \quad \Gamma_N, \end{cases} \tag{2.1}$$

with the interface conditions

$$\begin{cases} \boldsymbol{u}_f=\boldsymbol{u}_s=\dot{\boldsymbol{d}} & \text{on} \quad \Gamma,\\ \rho_s\epsilon\partial_t\dot{\boldsymbol{d}}+\boldsymbol{L}^e\boldsymbol{d}+\boldsymbol{L}^v\dot{\boldsymbol{d}}=-\sigma_f(\boldsymbol{u}_f,p_f)\boldsymbol{n} & \text{on} \quad \Gamma,\\ \boldsymbol{d}=\boldsymbol{0} & \text{on} \quad \partial\Gamma, \end{cases} \tag{2.2}$$

as well as the initial conditions

$$\boldsymbol{u}_f(0)=\boldsymbol{u}_f^0,\quad \boldsymbol{d}(0)=\boldsymbol{d}^0. \tag{2.3}$$

Here, ρ_f and ρ_s are the fluid density and the solid density respectively, ϵ is the solid thickness, $\dot{\boldsymbol{d}}$ is the solid velocity, $\boldsymbol{n}$ is the unit outer normal vector towards $\partial\Omega_f$,

$$\varepsilon(\boldsymbol{u}_f)=\frac{1}{2}(\nabla\boldsymbol{u}_f+\nabla\boldsymbol{u}_f^T),\quad \sigma_f(\boldsymbol{u}_f,p_f)=-p_f\boldsymbol{I}+2\mu_f\varepsilon(\boldsymbol{u}_f) \tag{2.4}$$

with μ_f being the fluid dynamic viscosity, $\boldsymbol{f}_N$ is a given surface force on Γ_N, $\boldsymbol{L}^e$ and $\boldsymbol{L}^v$ stand for the elastic and viscous contributions respectively.

The Dirichlet condition $(2.2)_1$ guarantees the continuity between the fluid velocity and the structure velocity at Γ while the Neumann condition $(2.2)_2$ ensures the continuity of the stresses at Γ. Note that equation $(2.2)_2$ is not only an interface coupling condition but also the structure governing equation in this model. The coupled model has been used extensively as a benchmark FSI model to examine the added-mass effects for decoupled methods.

Define

$$\begin{aligned} \boldsymbol{V}_f=\mathbf{H}_0^1(\Omega_f)&=\left\{\boldsymbol{u}_f\in(H^1(\Omega_f))^d \mid \boldsymbol{u}_f=0 \text{ on } \Gamma_D\right\},\\ \boldsymbol{V}_s=\mathbf{H}_0^1(\Omega_s)&=\left\{\boldsymbol{u}_s\in(H^1(\Gamma))^{d-1} \mid \boldsymbol{u}_s=0 \text{ on } \partial\Gamma\right\},\\ Q_f&=L^2(\Omega_f). \end{aligned} \tag{2.5}$$

Denote $\boldsymbol{V}\equiv\{(\boldsymbol{u}_f,\boldsymbol{u}_s)\in\boldsymbol{V}_f\times\boldsymbol{V}_s \mid \boldsymbol{u}_f|_\Gamma=\boldsymbol{u}_s|_\Gamma=\dot{\boldsymbol{d}}|_\Gamma\}$. The weak formulation of the coupled model reads as: finding $(\boldsymbol{u},p_f)\in\boldsymbol{V}\times Q_f$, and $\boldsymbol{d}\in\boldsymbol{V}_s$, such that $\boldsymbol{u}_s=\dot{\boldsymbol{d}}$ and

$$\begin{cases}(\delta_t\boldsymbol{u},\boldsymbol{v})+a_\Omega(\boldsymbol{u},\boldsymbol{v})+b(\boldsymbol{v},p_f)=f(\boldsymbol{v}),\ \forall\boldsymbol{v}\in\boldsymbol{V},\\ b(\boldsymbol{u},q)=0,\ \forall q\in Q_f,\end{cases}\tag{2.6}$$

satisfying the initial condition (2.3), where $\boldsymbol{u}\equiv(\boldsymbol{u}_f,\boldsymbol{u}_s)=(\boldsymbol{u}_f,\dot{\boldsymbol{d}})$, $\boldsymbol{v}\equiv(\boldsymbol{v}_f,\boldsymbol{v}_s)$, $\delta_t\boldsymbol{u}\equiv(\rho_f\frac{\partial\boldsymbol{u}_f}{\partial t}$, $\rho_s\epsilon\frac{\partial\boldsymbol{u}_s}{\partial t})$, $b(\boldsymbol{u},q)=-\int_{\Omega_f}q\mathrm{div}\boldsymbol{u}_f$, $a_\Omega(\boldsymbol{u},\boldsymbol{v})\equiv a_{\Omega_f}(\boldsymbol{u}_f,\boldsymbol{v}_f)+a_{\Omega_s}(\boldsymbol{d},\dot{\boldsymbol{d}},\boldsymbol{v}_s)$ with

$$a_{\Omega_f}(\boldsymbol{u}_f,\boldsymbol{v}_f)=2\int_{\Omega_f}\mu_f\varepsilon(\boldsymbol{u}_f):\varepsilon(\boldsymbol{v}_f)\quad\text{and}\quad a_{\Omega_s}(\boldsymbol{d},\dot{\boldsymbol{d}},\boldsymbol{v}_s)=\int_\Gamma\boldsymbol{L}_s(\boldsymbol{d},\dot{\boldsymbol{d}})\cdot\boldsymbol{v}_s.\tag{2.7}$$

Here and hereafter, we use $\boldsymbol{L}_s(\boldsymbol{d},\dot{\boldsymbol{d}})=\boldsymbol{L}^e+\boldsymbol{L}^v$ to denote the solid tensor. Note that, in (2.6), the Neumann interface condition is automatically guaranteed in the weak form, while the Dirichlet interface condition is enforced in the definition of $\boldsymbol{V}$.

3 Numerical Algorithms

3.1 The β Scheme

Algorithm 1: The β scheme.

For $m=0,1,2,3,...,N-1$,

1. Structure step: find $\tilde{\boldsymbol{u}}_s^{m+1}$ such that

$$\begin{cases}\rho_s\epsilon\frac{\tilde{\boldsymbol{u}}_s^{m+1}-\boldsymbol{u}_s^m}{\Delta t}+\boldsymbol{L}_s(\boldsymbol{d}^{m+1},\dot{\boldsymbol{d}}^{m+1})=-\beta\boldsymbol{\sigma}_f(\boldsymbol{u}_f^m,p_f^m)\boldsymbol{n} & \text{on }\Gamma,\\ \dot{\boldsymbol{d}}^{m+1}=\tilde{\boldsymbol{u}}_s^{m+1},\ \boldsymbol{d}^{m+1}=\boldsymbol{d}^m+\Delta t\tilde{\boldsymbol{u}}_s^{m+1} & \text{on }\Gamma.\end{cases}\tag{3.1}$$

2. Fluid step: find $\boldsymbol{u}_f^{m+1}$, p_f^{m+1} and $\boldsymbol{u}_s^{m+1}$ such that

$$\begin{cases}\frac{\rho_f}{\Delta t}(\boldsymbol{u}_f^{m+1}-\boldsymbol{u}_f^m)-\mathrm{div}\boldsymbol{\sigma}_f(\boldsymbol{u}_f^{m+1},p_f^{m+1})=\boldsymbol{0} & \text{in }\Omega_f,\\ \mathrm{div}\boldsymbol{u}_f^{m+1}=0, & \text{in }\Omega_f,\\ \rho_s\epsilon\frac{\boldsymbol{u}_s^{m+1}-\tilde{\boldsymbol{u}}_s^{m+1}}{\Delta t}=-\boldsymbol{\sigma}_f(\boldsymbol{u}_f^{m+1},p_f^{m+1})\boldsymbol{n}+\beta\boldsymbol{\sigma}_f(\boldsymbol{u}_f^m,p_f^m)\boldsymbol{n} & \text{on }\Gamma,\\ \boldsymbol{u}_f^{m+1}=\boldsymbol{u}_s^{m+1} & \text{on }\Gamma.\end{cases}\tag{3.2}$$

The β scheme proposed in [6] for approximating (2.6) is described in **Algorithm 1**, where the key is to split the structure equation as

$$\rho_s\epsilon\frac{\underbrace{\boldsymbol{u}_s^{m+1}-\tilde{\boldsymbol{u}}_s^{m+1}}+\tilde{\boldsymbol{u}}_s^{m+1}-\boldsymbol{u}_s^m}{\Delta t}+\boldsymbol{L}_s(\boldsymbol{d}^{m+1},\dot{\boldsymbol{d}}^{m+1})=$$
$$\underbrace{-\boldsymbol{\sigma}_f(\boldsymbol{u}_f^{m+1},p_f^{m+1})\boldsymbol{n}+\beta\boldsymbol{\sigma}_f(\boldsymbol{u}_f^m,p_f^m)\boldsymbol{n}}-\beta\boldsymbol{\sigma}_f(\boldsymbol{u}_f^m,p_f^m)\boldsymbol{n}.\tag{3.3}$$

The "$\underbrace{\quad}$" parts in (3.3) are then used in the fluid step as a Robin-type interface condition, whereas the other parts are computed in the structure step.

It is shown in [6] that the β scheme is stable if $\Delta t^2 \le Ch$ and $0 \le \beta \le 1$, and $\beta = 1$ leads to the optimal convergence. Therefore, we set $\beta = 1$ in our numerical experiments. We further note that when $\beta = 1$, the Robin-Neumann scheme [11] differs from the β scheme in which submodel being solved firstly. Comparisons between the Robin-Neumann scheme and the β scheme will be given in Section 4 by numerical experiments.

3.2 A Multirate β Scheme

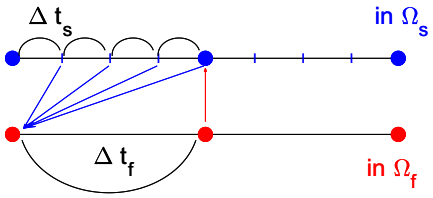

Figure 1: An illustration of a multirate time stepping technique.

Algorithm 2: A multirate β scheme.

For $k = 0,1,2,3,\ldots,N-1$, set $m_k = r \cdot k$,

1. Structure steps: for $m = m_k, m_k+1, m_k+2, \ldots, m_{k+1}-1$,

$$\begin{cases} \rho_s \epsilon \frac{\tilde{\boldsymbol{u}}_s^{m+1} - \boldsymbol{u}_s^m}{\Delta t_s} + \boldsymbol{L}_s(\boldsymbol{d}^{m+1}, \dot{\boldsymbol{d}}^{m+1}) = -\beta \sigma_f(\boldsymbol{u}_f^{m_k}, p_f^{m_k})\boldsymbol{n} & \text{on } \Gamma, \\ \dot{\boldsymbol{d}}^{m+1} = \tilde{\boldsymbol{u}}_s^{m+1}, \ \boldsymbol{d}^{m+1} = \boldsymbol{d}^m + \Delta t_s \tilde{\boldsymbol{u}}_s^{m+1} & \text{on } \Gamma. \end{cases} \tag{3.4}$$

2. Fluid step:

$$\begin{cases} \frac{\rho_f}{\Delta t_f}(\boldsymbol{u}_f^{m_{k+1}} - \boldsymbol{u}_f^{m_k}) - \mathrm{div}\,\sigma_f(\boldsymbol{u}_f^{m_{k+1}}, p_f^{m_{k+1}}) = \boldsymbol{0} & \text{in } \Omega_f, \\ \mathrm{div}\,\boldsymbol{u}_f^{m_{k+1}} = 0 & \text{in } \Omega_f, \\ \rho_s \epsilon \frac{\boldsymbol{u}_s^{m_{k+1}} - \tilde{\boldsymbol{u}}_s^{m_{k+1}}}{\Delta t_f} = -\sigma_f(\boldsymbol{u}_f^{m_{k+1}}, p_f^{m_{k+1}})\boldsymbol{n} + \beta \sigma_f(\boldsymbol{u}_f^{m_k}, p_f^{m_k})\boldsymbol{n} & \text{on } \Gamma, \\ \boldsymbol{u}_f^{m_{k+1}} = \boldsymbol{u}_s^{m_{k+1}} & \text{on } \Gamma. \end{cases} \tag{3.5}$$

To cope with the multi time-scale of the fluid and structure, we propose to apply the multirate time-stepping technique to the β scheme. The question is in which region the larger time step size should be used. Numerical experiments suggest that the version with a larger time step size in the fluid solver (cf. Figure 1) results in a better accuracy.

The corresponding method is described in **Algorithm** 2. We comment here that the multirate β scheme is nothing else but the β scheme itself when the time-step ratio $r=1$.

Algorithm 1 and **Algorithm 2** are the semi-discretization in the strong form. The corresponding fully discrete scheme with finite element discretization in space is described in **Algorithm** 3.

Algorithm 3: The fully discrete multirate β scheme.

For $k=0,1,2,3,...,N-1$, set $m_k=r\cdot k$

1. Structure step: for $m=m_k,m_k+1,m_k+2,...,m_{k+1}-1$, find $\tilde{\boldsymbol{u}}_{sh}^{m+1}\in\boldsymbol{V}_{sh}$ with $\dot{\boldsymbol{d}}_h^{m+1}=\tilde{\boldsymbol{u}}_{sh}^{m+1}$ and $\boldsymbol{d}_h^{m+1}=\boldsymbol{d}_h^m+\Delta t_s\tilde{\boldsymbol{u}}_{sh}^{m+1}$, such that $\forall\boldsymbol{v}_{sh}\in\boldsymbol{V}_{sh}$, there holds

$$\rho_s\epsilon\left(\frac{\tilde{\boldsymbol{u}}_{sh}^{m+1}-\boldsymbol{u}_{sh}^m}{\Delta t_s},\boldsymbol{v}_{sh}\right)_\Gamma+a_{\Omega_s}(\boldsymbol{d}_h^{m+1},\dot{\boldsymbol{d}}_h^{m+1},\boldsymbol{v}_{sh})=-\beta\left(\boldsymbol{\sigma}_f(\boldsymbol{u}_{fh}^{m_k},p_{fh}^{m_k})\boldsymbol{n},\boldsymbol{v}_{sh}\right)_\Gamma. \tag{3.6}$$

2. Fluid step: find $(\boldsymbol{u}_{fh}^{m_{k+1}},\boldsymbol{u}_{sh}^{m_{k+1}},p_{fh}^{m_{k+1}})\in(\boldsymbol{V}_{fh},\boldsymbol{V}_{sh},Q_{fh})$ with $\boldsymbol{u}_{fh}^{m_{k+1}}|_\Gamma=\boldsymbol{u}_{sh}^{m_{k+1}}$ such that $\forall(\boldsymbol{v}_{fh},\boldsymbol{v}_{sh},q_{fh})\in(\boldsymbol{V}_{fh},\boldsymbol{V}_{sh},Q_{fh})$ with $\boldsymbol{v}_{fh}|_\Gamma=\boldsymbol{v}_{sh}$, there holds

$$\begin{aligned}\rho_f\left(\frac{\boldsymbol{u}_{fh}^{m_{k+1}}-\boldsymbol{u}_{fh}^{m_k}}{\Delta t_f},\boldsymbol{v}_{fh}\right)_\Omega&+a_{\Omega_f}(\boldsymbol{u}_{fh}^{m_{k+1}},\boldsymbol{v}_{fh})-b(p_{fh}^{m_{k+1}},\boldsymbol{v}_{fh})+b(q_{fh},\boldsymbol{u}_{fh}^{m_{k+1}})\\&+\rho_s\epsilon\left(\frac{\boldsymbol{u}_{sh}^{m_{k+1}}-\tilde{\boldsymbol{u}}_{sh}^{m_{k+1}}}{\Delta t_f},\boldsymbol{v}_{sh}\right)_\Gamma=\beta\left(\boldsymbol{\sigma}_f(\boldsymbol{u}_{fh}^{m_k},p_{fh}^{m_k})\boldsymbol{n},\boldsymbol{v}_{sh}\right)_\Gamma.\end{aligned} \tag{3.7}$$

Remark 3.1. In the multirate β scheme, if $m=m_k$, we have $\boldsymbol{u}_s^m=\boldsymbol{u}_s^{m_k}$ from the fluid step, and if $m>m_k$, we take $\boldsymbol{u}_s^m=\tilde{\boldsymbol{u}}_s^m$ from the structure step.

4 Numerical Experiments and Simulation

4.1 Numerical Experiments for the Fluid and Thin-walled Structure Model

In this subsection, we present numerical experiments to demonstrate the convergence and stability performance of the multirate β scheme (3.6)-(3.7) for coupling a Stokes flow with a thin-walled structure by using a benchmark model. The model consists of a *2-D* rectangular fluid domain $\Omega_f=[0,L]\times[0,R]$ with $L=6$ and $R=0.5$ and a *1-D* structure domain $\Gamma=[0,L]\times R$ that meanwhile also plays the role of the fluid-solid interface, as shown in **Figure 2**. The displacement of the interface is assumed to be infinitesimal and the Reynolds number in the fluid is assumed to be small. All the quantities will be given in terms of the centimeter-gram-second (CGS) system of units.

The physical parameters are set as follows: $\rho_f=1.0$, $\rho_s=1.1$, $\mu=0.035$; $\boldsymbol{L}_s(\boldsymbol{d},\dot{\boldsymbol{d}})=c_1\partial_x^2\boldsymbol{d}+c_0\boldsymbol{d}$, where $c_1=\frac{E\epsilon}{2(1+\nu)}$, $c_0=\frac{E\epsilon}{R^2(1-\nu^2)}$ with $\epsilon=0.1$, the Poisson ratio $\nu=0.5$ and the

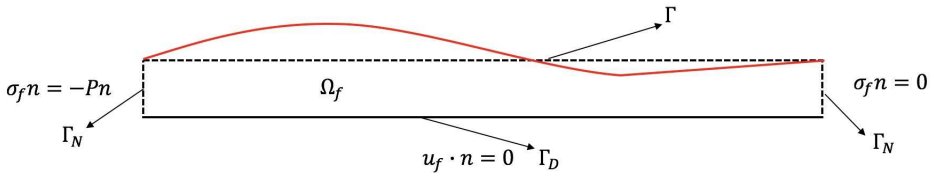

Figure 2: Geometrical configuration.

Young's modulus $E = 0.75 \cdot 10^6$. A pressure-wave

$$P(t) = P_{max}(1 - \cos(2t\pi/T^*))/2 \quad \text{with} \quad P_{max} = 2 \cdot 10^4,$$

is prescribed on the fluid inlet boundary for $T^* = 5 \cdot 10^{-3}$ (seconds). Zero traction is enforced on the fluid outlet boundary and no-slip condition is imposed on the lower boundary $y = 0$. For the solid, the two endpoints are fixed with $\boldsymbol{d} = \mathbf{0}$ at $x = 0$ and $x = 6$.

The first experiment is set up to compare the Robin-Neumann scheme with the β scheme, the two stable decoupled methods recently developed for the benchmark model. Figure 3 displays the displacements computed by the Robin-Neumann scheme and the β scheme, together with the coupled implicit scheme for reference, where the mesh size and the time step size are $h = 0.05$ and $\Delta t = 10^{-4}$. It is clearly seen that both decoupled schemes converge as well as the coupled implicit scheme. Moreover, little difference is observed between the two decoupled schemes numerically. This suggests us to focus on the β scheme for investigating the multirate time-step technique.

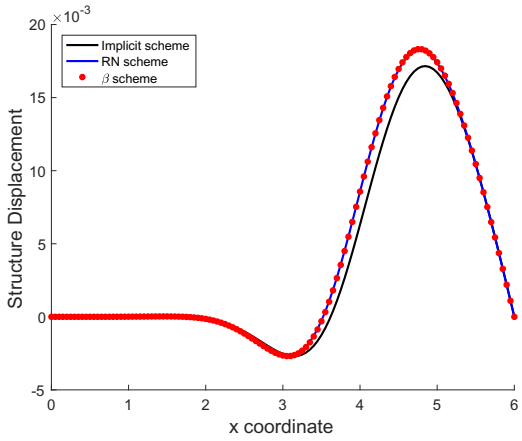

Figure 3: Comparisons of the numerical results obtained by the coupled implicit scheme, the RN scheme, and the β scheme under the setting: $h = 0.05$ and $\Delta t_s = 10^{-4}$.

We then conduct numerical experiments to investigate the effects of the time-step ratio r. Figure 4 illustrates that a larger time step size in the fluid part results in a more accurate numerical solution than that obtained by using a larger step size in the structure part. In the test, we fix $h = 0.1$ and $\Delta t = 10^{-5}$. In addition, we observe that, when $\frac{\Delta t_s}{\Delta t_f}$

is further increased to be $\frac{\Delta t_s}{\Delta t_f} = 5$ or $\frac{\Delta t_s}{\Delta t_f} = 10$, there are substantial numerical instability. This screens out the possibility of using a larger time step size in the structure part.

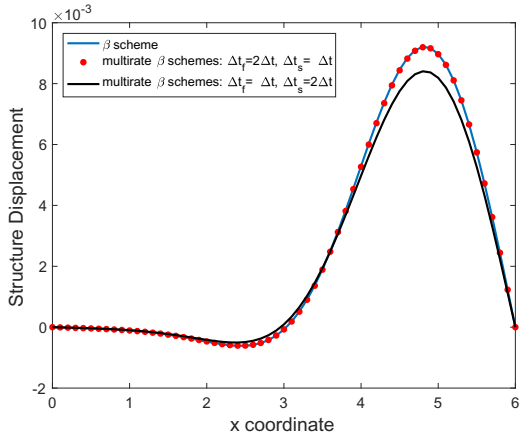

Figure 4: Comparison of the β scheme and the multirate β schemes with two different time-step ratios ($h = 0.1$ and $\Delta t = 10^{-5}$ are fixed).

To examine how the stability and approximation are affected when the time step in the fluid region is too large, we fix the time step Δt_s and h while vary the time-step ratio $r = 1,5,10,20,50$. Figure 5 displays the computed displacements at $t = 0.015$ with the structure time step size $\Delta t_s = 10^{-5}$, the mesh size $h = 0.1$ (left) and $h = 0.01$ (right). In the left figure, we observe that the structure displacements computed by using $r = 1$, 2, 5,10 approximate very well to that by using the coupled implicit scheme. To further investigate the stability and the convergence of the multirate β scheme, in the right part of Figure 5, we reduce the mesh size to be $h = 0.01$ while fixing the time step size. The numerical results confirm that the multirate β scheme is still stable even the time-step ratio is reasonably large.

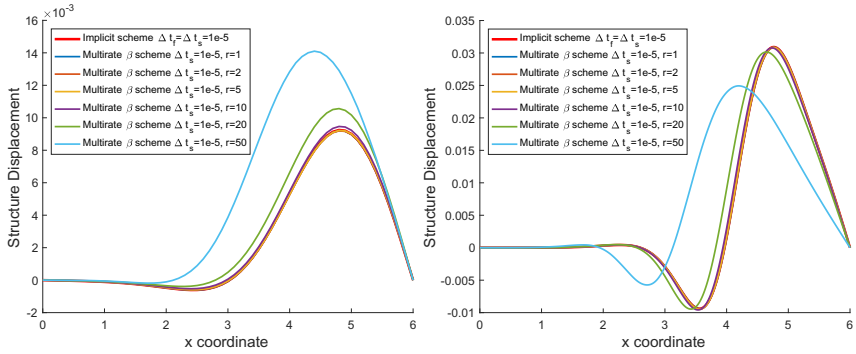

Figure 5: Numerical displacements under the settings: $h = 0.1$ (left) $h = 0.01$ (right) and $\Delta t_s = 10^{-5}$.

In Figure 6, we present the numerical results of the fluid pressure distribution at $t=0.005$, 0.01, 0.015. From the top to the bottom, numerical results are: a reference solution by the coupled implicit scheme, the numerical solution by the β scheme, and the solution by the multirate β scheme with $r=10$. By comparing the results, we see that the multirate β scheme provides a very good approximation.

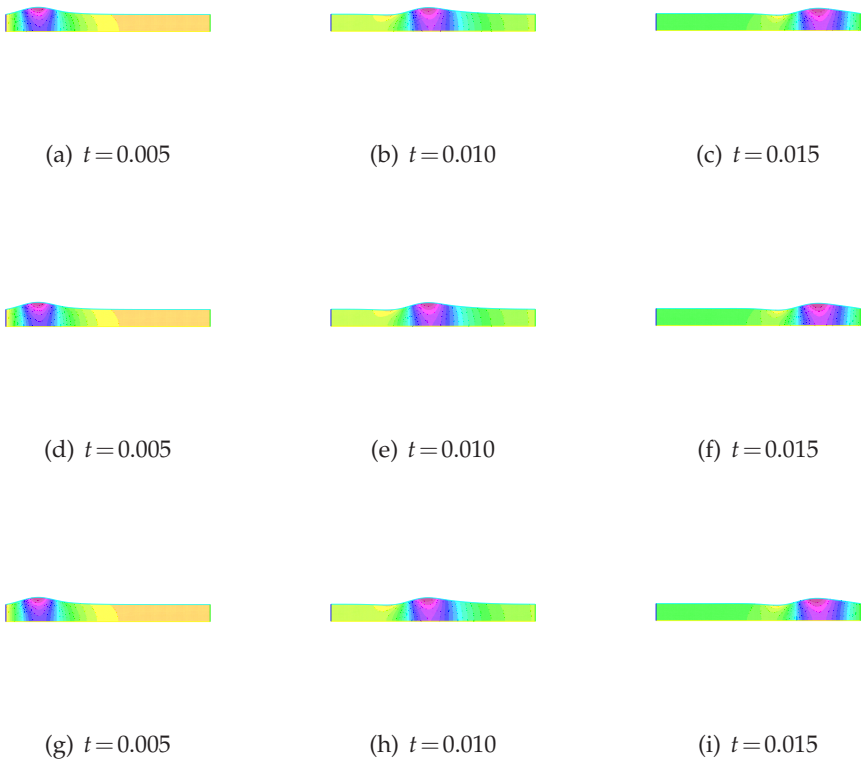

(a) $t=0.005$ (b) $t=0.010$ (c) $t=0.015$

(d) $t=0.005$ (e) $t=0.010$ (f) $t=0.015$

(g) $t=0.005$ (h) $t=0.010$ (i) $t=0.015$

Figure 6: Fluid pressure distribution at $t=0.005$, 0.010, 0.015 obtained by the coupled implicit scheme (top), the multirate β scheme with $r=1$ (middle) and $r=10$ (bottom) with $h=0.01$ and $\Delta t_s=0.00001$.

In order to examine the order of convergence, we start with $h=0.1$ and $\Delta t_s=0.0001$, and then refine the mesh size by a factor of 2 and the time step size by a factor of 4. The space-time size settings are:

$$\{h,\Delta t_s\}^i=\{0.1\cdot(0.5)^i,0.0001\cdot(0.25)^i\},\ \ i=0,1,2,3,4. \tag{4.1}$$

We compare the numerical solutions of the multirate β scheme with the reference solution. The reference solution is computed by using the coupled implicit scheme with a high space-time grid resolution ($h=3.125\times10^{-3}$, $\Delta t=10^{-6}$) as that in [11]. In the multirate scheme, $r=1$ and $r=10$. The relative errors of the primary variables ($\boldsymbol{u}_f$, p_f

and $\boldsymbol{d}$) at $t = 0.015$ are displayed in Figure 7. From the comparisons, we see that the numerical errors are approximately reduced by a factor of 4 as the mesh size and the time step size are refined once. Therefore, the multirate β scheme is of a second order in h and a first order in t.

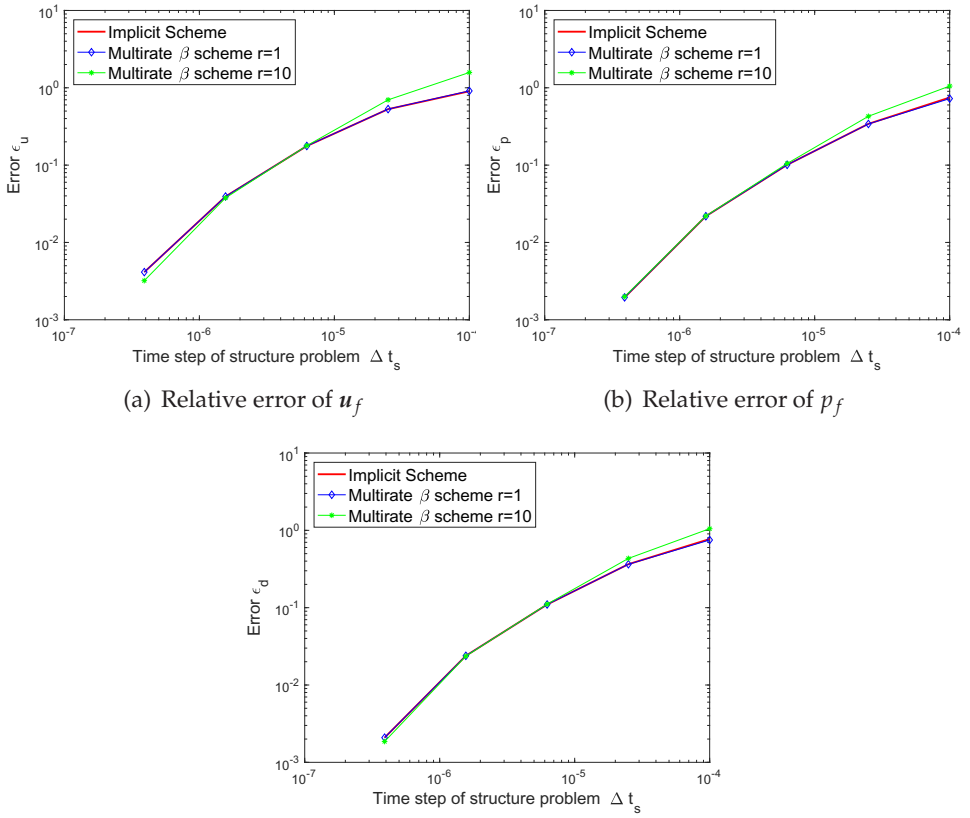

(a) Relative error of $\boldsymbol{u}_f$

(b) Relative error of p_f

(c) Relative error of $\boldsymbol{d}$

Figure 7: Relative errors of primary variables with the spacing h and time step size Δt_s in (4.1).

Finally, in order to demonstrate the advantage of the multirate β scheme, we compare in Table 1 the CPU times of the concerned numerical algorithms under various settings. We fixed $\Delta t_s = 10^{-5}$ and vary the mesh sizes as $h = \frac{1}{10}, \frac{1}{20}, \frac{1}{40}, \frac{1}{80}, \frac{1}{160}$. From the table, it is observed that the multirate β scheme takes much less computational cost than that of the coupled implicit scheme, particularly when r is large.

Table 1: CPU times (in seconds) for the coupled implicit scheme and the multirate β scheme (with $r=1$ or 10) under different settings of mesh sizes ($\Delta t_s = 10^{-5}$ is fixed).

	Implicit Scheme	Multirate β scheme r=1	Multirate β scheme r=10
$h=\frac{1}{10}$	14.90	4.02	0.74
$h=\frac{1}{20}$	48.64	16.00	2.82
$h=\frac{1}{40}$	179.83	66.67	11.6
$h=\frac{1}{80}$	797.76	297.96	49.23
$h=\frac{1}{160}$	3165.26	1270.30	206.32

4.2 Extension to More General Settings

In this subsection, we demonstrate that the multirate β scheme can be naturally extended to FSI applications with nonlinear models, complex geometric domains, and large structural deformations. We use $\Omega_f(t)\subset\mathbb{R}^d$ and $\Omega_s(t)\subset\mathbb{R}^d$ to represent current domains of fluid flow and the structure, respectively. The boundaries of the domains are denoted by $\Gamma_f(t)$ and $\Gamma_s(t)$. Denote the interface between the fluid flow and structure by $\Gamma_I(t)=\Gamma_f(t)\cap\Gamma_s(t)$. In order to distinguish the reference domain from the current one, we use the notation "$\hat{}$" to denote the reference domains and boundaries: $\hat{\Omega}_f=\Omega_f(0)$, $\hat{\Omega}_s=\Omega_s(0)$ and $\hat{\Gamma}_f=\Gamma_f(0)$, $\hat{\Gamma}_s=\Gamma_s(0)$, $\hat{\Gamma}_I=\Gamma_I(0)$. For simplification, we omit the temporal variable t in the definitions of domains and boundaries in the rest of this paper. For any point $\hat{\boldsymbol{x}}\in\hat{\Omega}=\hat{\Omega}_f\cup\hat{\Omega}_s$, the position at t is denoted by $\boldsymbol{x}(\hat{\boldsymbol{x}},t)\in\Omega=\Omega_f\cup\Omega_s$. The variables in the reference domain with Lagrangian coordinates are: the displacement $\hat{\boldsymbol{d}}(\hat{\boldsymbol{x}},t)=\boldsymbol{x}-\hat{\boldsymbol{x}}$ and the velocity $\hat{\boldsymbol{u}}(\hat{\boldsymbol{x}},t)=\partial_t\hat{\boldsymbol{d}}(\hat{\boldsymbol{x}},t)$. Because of the relation $\boldsymbol{x}=\hat{\boldsymbol{x}}+\hat{\boldsymbol{d}}(\hat{\boldsymbol{x}},t)$, the velocity with Eulerian coordinates is defined by $\boldsymbol{u}(\boldsymbol{x},t)=\partial_t\boldsymbol{x}=\partial_t\hat{\boldsymbol{d}}(\hat{\boldsymbol{x}},t)=\hat{\boldsymbol{u}}(\hat{\boldsymbol{x}},t)$.

The fluid motion is described by the incompressible Navier-Stokes equations in the Eulerian coordinates:

$$\rho_f D_t\boldsymbol{u}_f-\nabla\cdot\boldsymbol{\sigma}_f = \boldsymbol{f}_f \quad \text{in } \Omega_f, \tag{4.2}$$

$$\nabla\cdot\boldsymbol{u}_f = 0 \quad \text{in } \Omega_f. \tag{4.3}$$

Here, σ_f is defined as in (2.4) and $\boldsymbol{f}_f$ is the body force. $D_t\boldsymbol{u}_f$ is the total derivative, which is defined in (4.9) later. The structure is modeled by an elastic equation in Lagrangian coordinates for the displacement $\hat{\boldsymbol{d}}_s$:

$$\hat{\rho}_s\partial_{tt}\hat{\boldsymbol{d}}_s-\nabla_{\hat{\boldsymbol{x}}}\cdot\boldsymbol{P}_s=\hat{\boldsymbol{f}}_s \quad \text{in } \hat{\Omega}_s. \tag{4.4}$$

In (4.4), the first Piola stress $\boldsymbol{P}_s$ is described as

$$\boldsymbol{P}_s=J\boldsymbol{\sigma}_s\boldsymbol{F}^{-\mathrm{T}}, \tag{4.5}$$

and the Cauchy stress tensor is $\boldsymbol{\sigma}_s=2\mu\varepsilon(\hat{\boldsymbol{d}}_s)+\lambda\mathrm{div}\hat{\boldsymbol{d}}_s$ with μ being the shear modulus and λ being the Lamé parameter. $\boldsymbol{F}=\mathbf{I}+\nabla_{\hat{\boldsymbol{x}}}\hat{\boldsymbol{d}}_s$ is the deformation gradient tensor and

$J=|\boldsymbol{F}|$. Both the velocity and the normal stress are continuous across the interface, which can be defined as interface conditions in the Eulerian coordinates as follows

$$\begin{cases} \boldsymbol{\sigma}_s\boldsymbol{n}=\boldsymbol{\sigma}_f\boldsymbol{n} & \text{on } \Gamma_I, \\ \boldsymbol{u}_s=\boldsymbol{u}_f & \text{on } \Gamma_I. \end{cases} \tag{4.6}$$

The arbitrary Lagrangian−Eulerian (ALE) method is needed to deal with the moving domains. Denote the ALE mapping $\mathcal{A}$ as

$$\begin{aligned} \mathcal{A}=\mathcal{A}_f^t:\hat{\Omega}_f\mapsto\Omega_f,\ \ \forall t\geq 0, \\ \boldsymbol{x}=\mathcal{A}_f^t(\boldsymbol{x}_0)=\boldsymbol{x}_0+\mathbf{Ext}(\hat{\boldsymbol{d}}_s(\boldsymbol{x}_0,t)|_{\hat{\Gamma}_I}). \end{aligned} \tag{4.7}$$

Here, $\mathbf{Ext}(\cdot)$ is an appropriate extension of the structure displacement at the interface. A classical choice of the extension is the harmonic extension defined by

$$\begin{cases} \Delta\hat{\boldsymbol{d}}_m=0 & \text{in } \hat{\Omega}_f, \\ \hat{\boldsymbol{d}}_m=0 & \text{on } \hat{\Gamma}_f\backslash\hat{\Gamma}_I, \\ \hat{\boldsymbol{d}}_m=\hat{\boldsymbol{d}}_s & \text{on } \hat{\Gamma}_I. \end{cases} \tag{4.8}$$

In (4.8), $\hat{\boldsymbol{d}}_m$ is actually the displacement of the mesh. The time derivative of the moving grid is

$$D_t\boldsymbol{u}_f=\partial_t^{\mathcal{A}}\boldsymbol{u}_f+(\boldsymbol{u}_f-\boldsymbol{u}_m)\cdot\nabla\boldsymbol{u}_f. \tag{4.9}$$

Here, $\partial_t^{\mathcal{A}}$ is the ALE time derivative and $\boldsymbol{u}_m$ denotes the velocity of the mesh, which can be calculated by

$$\boldsymbol{u}_m(\boldsymbol{x},t)=\partial_t\boldsymbol{x}|_{\boldsymbol{x}_0}=\partial_t(\boldsymbol{x}_0+\mathbf{Ext}(\hat{\boldsymbol{d}}_s(\boldsymbol{x}_0,t)|_{\hat{\Gamma}_I})=\partial_t\hat{\boldsymbol{d}}_m(\hat{\boldsymbol{x}},t). \tag{4.10}$$

After introducing the ALE mapping, the FSI model reads as: finding $\boldsymbol{u}_f,p_f,\hat{\boldsymbol{u}}_s$ such that

$$\begin{cases} \rho_f(\partial_t^{\mathcal{A}}\boldsymbol{u}_f+(\boldsymbol{u}_f-\boldsymbol{u}_m)\cdot\nabla\boldsymbol{u}_f)-\nabla\cdot\boldsymbol{\sigma}_f=\boldsymbol{f}_f & \text{in } \Omega_f, \\ \nabla\cdot\boldsymbol{u}_f=0 & \text{in } \Omega_f, \\ \hat{\rho}_s\partial_{tt}\hat{\boldsymbol{d}}_s-\nabla_{\hat{x}}\cdot\boldsymbol{P}_s=\hat{\boldsymbol{f}}_s & \text{in } \hat{\Omega}_s. \end{cases} \tag{4.11}$$

The complete FSI model also includes the initial and boundary conditions

$$\begin{cases} \boldsymbol{u}_f(\boldsymbol{x},0)=0 \ \ \text{in } \Omega_f,\ \ \hat{\boldsymbol{u}}_s(\hat{\boldsymbol{x}},0)=0 \ \ \text{in } \hat{\Omega}_s, \\ \boldsymbol{u}_f=\boldsymbol{u}_{f,D} \ \ \text{on } \Gamma_{f,D},\ \ \hat{\boldsymbol{u}}_s=\hat{\boldsymbol{u}}_{s,D} \ \ \text{on } \hat{\Gamma}_{s,D}, \\ \boldsymbol{\sigma}_f\boldsymbol{n}=\boldsymbol{g}_{f,N} \ \ \text{on } \Gamma_{f,N},\ \ \boldsymbol{P}_s\boldsymbol{n}=\hat{\boldsymbol{g}}_{s,N} \ \ \text{on } \hat{\Gamma}_{s,N}, \end{cases} \tag{4.12}$$

the constitutive relations (2.4), (4.5), the ALE mapping relations (4.7), (4.8), (4.10) and the interface conditions (4.6).

Define

$$\begin{aligned} \hat{\boldsymbol{V}}_s=\mathbf{H}_0^1(\hat{\Omega}_s)=\left\{\hat{\boldsymbol{u}}_s\in(H^1(\hat{\Omega}_s))^d \mid \hat{\boldsymbol{u}}_s=0 \text{ on } \hat{\Gamma}_{s,D}\right\}, \\ \hat{\boldsymbol{V}}_m=\mathbf{H}_0^1(\hat{\Omega}_f)=\left\{\hat{\boldsymbol{d}}_m\in(H^1(\hat{\Omega}_f))^d \mid \hat{\boldsymbol{d}}_m=0 \text{ on } \hat{\Gamma}_f\backslash\hat{\Gamma}_I\right\}. \end{aligned} \tag{4.13}$$

Then, denote $\boldsymbol{W}=\left\{(\boldsymbol{u}_f,\hat{\boldsymbol{u}}_s)\in\boldsymbol{V}_f\times\hat{\boldsymbol{V}}_s \mid \boldsymbol{u}_f=\hat{\boldsymbol{u}}_s\circ\hat{\boldsymbol{x}}(\boldsymbol{x},t) \text{ on } \Gamma_I\right\}$. We adopt $P1-P1$ finite elements with a SUPG/PSPG stabilized formulation [28] for the fluid problem, and apply $P1$ elements for both the structure problem and the ALE mapping. The general version of the multirate β scheme is described in Algorithm 4.

Algorithm 4: The fully discrete multirate β scheme (a general version).

For $k=0,1,2,3,...,N-1$, set $m_k=r\cdot k$

1. Structure step: for $m=m_k,m_k+1,m_k+2,...,m_{k+1}-1$, find $\left(\tilde{\boldsymbol{u}}_{fh}^{m+1},\tilde{\hat{\boldsymbol{u}}}_{sh}^{m+1}\right)\in\boldsymbol{W}_h$ with $\hat{\boldsymbol{d}}_{sh}^{m+1}=\hat{\boldsymbol{d}}_{sh}^{m}+\Delta t_s\tilde{\hat{\boldsymbol{u}}}_{sh}^{m+1}$ such that $\forall\left(\boldsymbol{v}_{fh},\hat{\boldsymbol{v}}_{sh}\right)\in\boldsymbol{W}_h$, there holds

$$\begin{aligned}\hat{\rho}_s\left(\frac{\tilde{\hat{\boldsymbol{u}}}_{sh}^{m+1}-\hat{\boldsymbol{u}}_{sh}^{m}}{\Delta t_s},\hat{\boldsymbol{v}}_{sh}\right)_{\hat{\Omega}_s}+\left(\boldsymbol{P}_s(\hat{\boldsymbol{d}}_{sh}^{m+1}),\hat{\boldsymbol{v}}_{sh}\right)_{\hat{\Omega}_s}+\rho_f\left(\frac{\tilde{\boldsymbol{u}}_{fh}^{m+1}-\boldsymbol{u}_{fh}^{m_k}}{\Delta t_f},\boldsymbol{v}_{fh}\right)_{\Omega_f}&\\ =-\beta\left(\boldsymbol{\sigma}_f(\boldsymbol{u}_{fh}^{m_k},p_{fh}^{m_k})\boldsymbol{n},\boldsymbol{v}_{fh}\right)_{\Gamma_I}.&\end{aligned}\tag{4.14}$$

2. Update mesh: find $\hat{\boldsymbol{d}}_{mh}^{m_{k+1}}\in\hat{\boldsymbol{V}}_{mh}$ with $\hat{\boldsymbol{d}}_{mh}^{m_{k+1}}|_{\hat{\Gamma}_I}=\hat{\boldsymbol{d}}_{sh}^{m_{k+1}}|_{\hat{\Gamma}_I}$ such that $\forall\hat{\boldsymbol{v}}_{mh}\in\hat{\boldsymbol{V}}_{mh}$, there holds

$$\left(\nabla\hat{\boldsymbol{d}}_{mh}^{m_{k+1}},\nabla\hat{\boldsymbol{v}}_{mh}\right)_{\hat{\Omega}_f}=0.\tag{4.15}$$

Then the fluid domain is updated by $\Omega_f=\hat{\Omega}_f+\hat{\boldsymbol{d}}_{mh}^{m_{k+1}}$, and $\boldsymbol{u}_{mh}^{m_{k+1}}$ is calculated by (4.10).

3. Fluid step: find $((\boldsymbol{u}_{fh}^{m_{k+1}},\hat{\boldsymbol{u}}_{sh}^{m_{k+1}}),p_{fh}^{m_{k+1}})\in(\boldsymbol{W}_h,Q_{fh})$ such that $\forall((\boldsymbol{v}_{fh},\hat{\boldsymbol{v}}_{sh}),q_{fh})\in(\boldsymbol{W}_h,Q_{fh})$, there holds

$$\begin{aligned}&\rho_f\left(\frac{\boldsymbol{u}_{fh}^{m_{k+1}}-\tilde{\boldsymbol{u}}_{fh}^{m_{k+1}}}{\Delta t_f},\boldsymbol{v}_{fh}\right)_{\Omega_f}+\left(\rho_f(\boldsymbol{u}_{fh}^{m_{k+1}}-\boldsymbol{u}_{mh}^{m_{k+1}})\cdot\nabla\boldsymbol{u}_{fh}^{m_{k+1}},\boldsymbol{v}_{fh}\right)_{\Omega_f}+a_{\Omega_f}(\boldsymbol{u}_{fh}^{m_{k+1}},\boldsymbol{v}_{fh})\\ &-b(p_{fh}^{m_{k+1}},\boldsymbol{v}_{fh})+b(q_{fh},\boldsymbol{u}_{fh}^{m_{k+1}})+\hat{\rho}_s\left(\frac{\hat{\boldsymbol{u}}_{sh}^{m_{k+1}}-\tilde{\hat{\boldsymbol{u}}}_{sh}^{m_{k+1}}}{\Delta t_s},\hat{\boldsymbol{v}}_{sh}\right)_{\hat{\Omega}_s}=\beta\left(\boldsymbol{\sigma}_f(\boldsymbol{u}_{fh}^{m_k},p_{fh}^{m_k})\boldsymbol{n},\boldsymbol{v}_{fh}\right)_{\Gamma_I}.\end{aligned}\tag{4.16}$$

We consider a FSI numerical example for studying the abdominal aneurysm [14]. The *2-D*$\times$*2-D* unsymmetrical computational domain is shown in the left part of Figure 8. The length of this domain L is 0.08 m, the thickness of the structure ϵ is 0.002 m and the radius of the fluid inlet r is 0.01 m. The physical parameters are described as: $\rho_f=1.060\times10^3\ kg/m^3$, $\mu_f=3.7\cdot10^{-3}\ Pa\times s$; $\hat{\rho}_s=1.15\times10^3\ kg/m^3$, $\mu=1.80645\times10^5$,

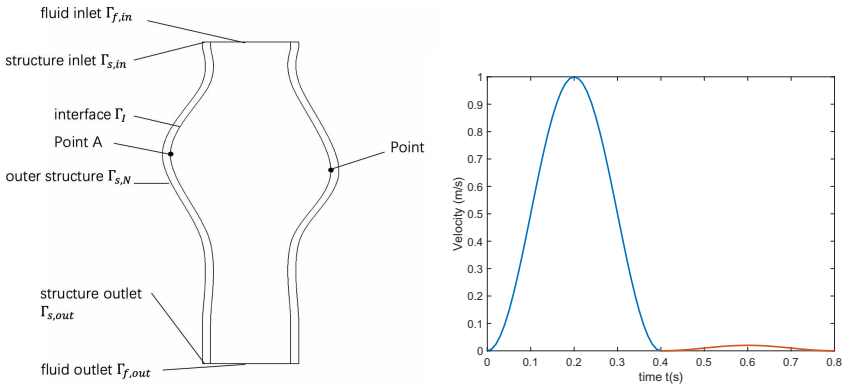

Figure 8: Computational domain (left) and inlet flow $\bar{\boldsymbol{u}}_{in}(t)$ (right).

$\lambda = 5.9797 \times 10^5$. Define

$$\bar{\boldsymbol{u}}_{in}(t) = \begin{cases} 1\left(\sin(\dfrac{2\pi}{0.4}t - \dfrac{\pi}{2}) + 1\right)/2, & t \in [0, 0.4], \\ 0.02\left(\sin(\dfrac{2\pi}{0.4}(t-0.4) - \dfrac{\pi}{2}) + 1\right)/2, & t \in [0.4, 0.8]. \end{cases} \tag{4.17}$$

The time dependent function (4.17) is an approximation of the blood inlet flow in $0.8s$ cardiac cycle (see the right part of Figure 8 for its profile). We impose the Dirichlet condition on the fluid inlet boundary by using $\boldsymbol{u}_{in}(\boldsymbol{x},t) = \bar{\boldsymbol{u}}_{in}(t) \cdot (r^2 - \|\boldsymbol{x} - \boldsymbol{x}_0\|_2^2)/r^2$, where $\boldsymbol{x}_0$ is the center of the fluid inlet and x is any point on the fluid inlet boundary. The complete boundary conditions for such a biomechanical test are as follows.

$$\begin{cases} \boldsymbol{u}_f = \boldsymbol{u}_{in} \quad \text{on } \Gamma_{f,in}, \ \hat{\boldsymbol{u}}_s = \boldsymbol{0} \quad \text{on } \hat{\Gamma}_{s,in} \cup \hat{\Gamma}_{s,out}, \\ \boldsymbol{\sigma}_f \boldsymbol{n} = \boldsymbol{0} \quad \text{on } \Gamma_{f,out}, \ \boldsymbol{P}_s \boldsymbol{n} = \boldsymbol{0} \quad \text{on } \hat{\Gamma}_{s,N}. \end{cases}$$

To validate the efficiency of the multirate β scheme, similar to Table 1, we have two setups of discretization parameters: (1) a coarse mesh with 1966 triangular elements and $\Delta t_s = 0.001$; (2) a fine mesh with 7864 triangular elements and $\Delta t_s = 0.0001$. In order to measure the movement of the interface, we present the displacement magnitudes of Point A and Point B in Figure 9 and Figure 10, in which the results of the coupled implicit scheme, the multirate β scheme with $r = 1$ and $r = 10$ are compared. The coarse mesh and $\Delta t_s = 0.001$ are used in Figure 9 whereas the fine mesh and $\Delta t_s = 0.0001$ are used in Figure 10. We also show the velocity distributions at $t = 0.2,\ 0.4,\ 0.6,\ 0.8\ s$ obtained by the coupled implicit scheme, the multirate β scheme with $r = 1$ and $r = 10$ on the fine mesh and fixing $\Delta t_s = 0.0001$ in Figure 11. From these figures, we see clearly that the multirate β scheme produces comparable numerical results as that of the coupled implicit scheme. Furthermore, for the two discretization setups, the CPU times for the multirate β scheme with $r = 10$ are around $\frac{1}{6}$ of that for the scheme with $r = 1$. Therefore, the multirate scheme improves the efficiency substantially.

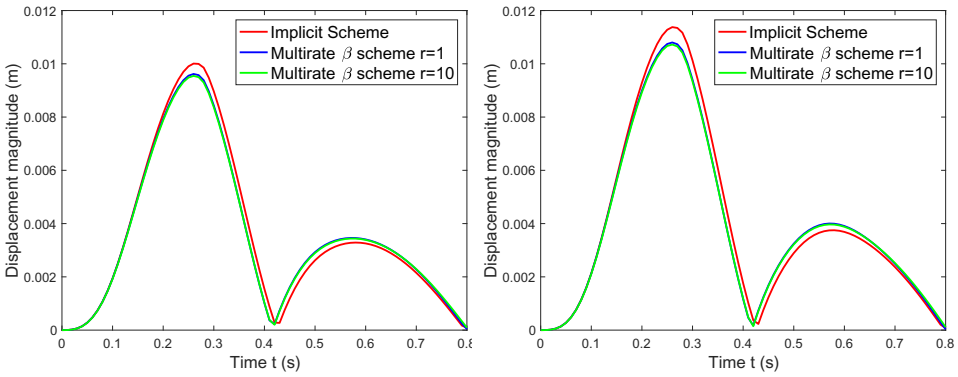

Figure 9: Displacement magnitudes of Point A (left) and Point B (right) in 0.8 s obtained by the coupled implicit scheme, the multirate β scheme with $r = 1$ and $r = 10$ with a coarse mesh and $\Delta t_s = 0.001$.

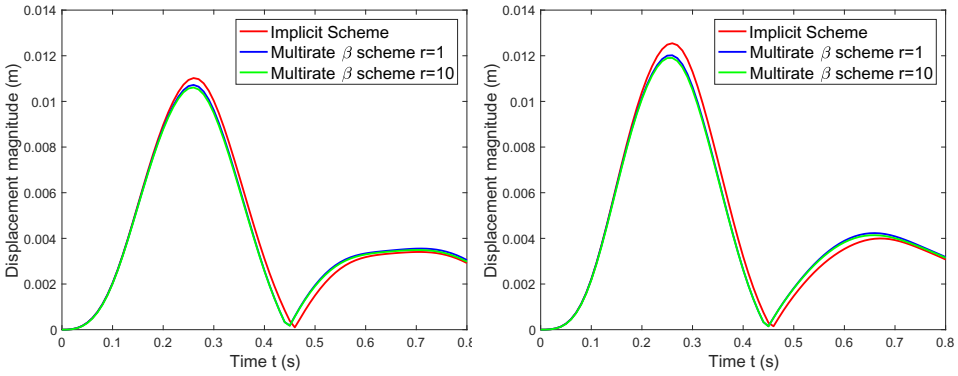

Figure 10: Displacement magnitudes of Point A (left) and Point B (right) in 0.8 s obtained by the coupled implicit scheme, the multirate β scheme with $r = 1$ and $r = 10$ with a fine mesh and $\Delta t_s = 0.0001$.

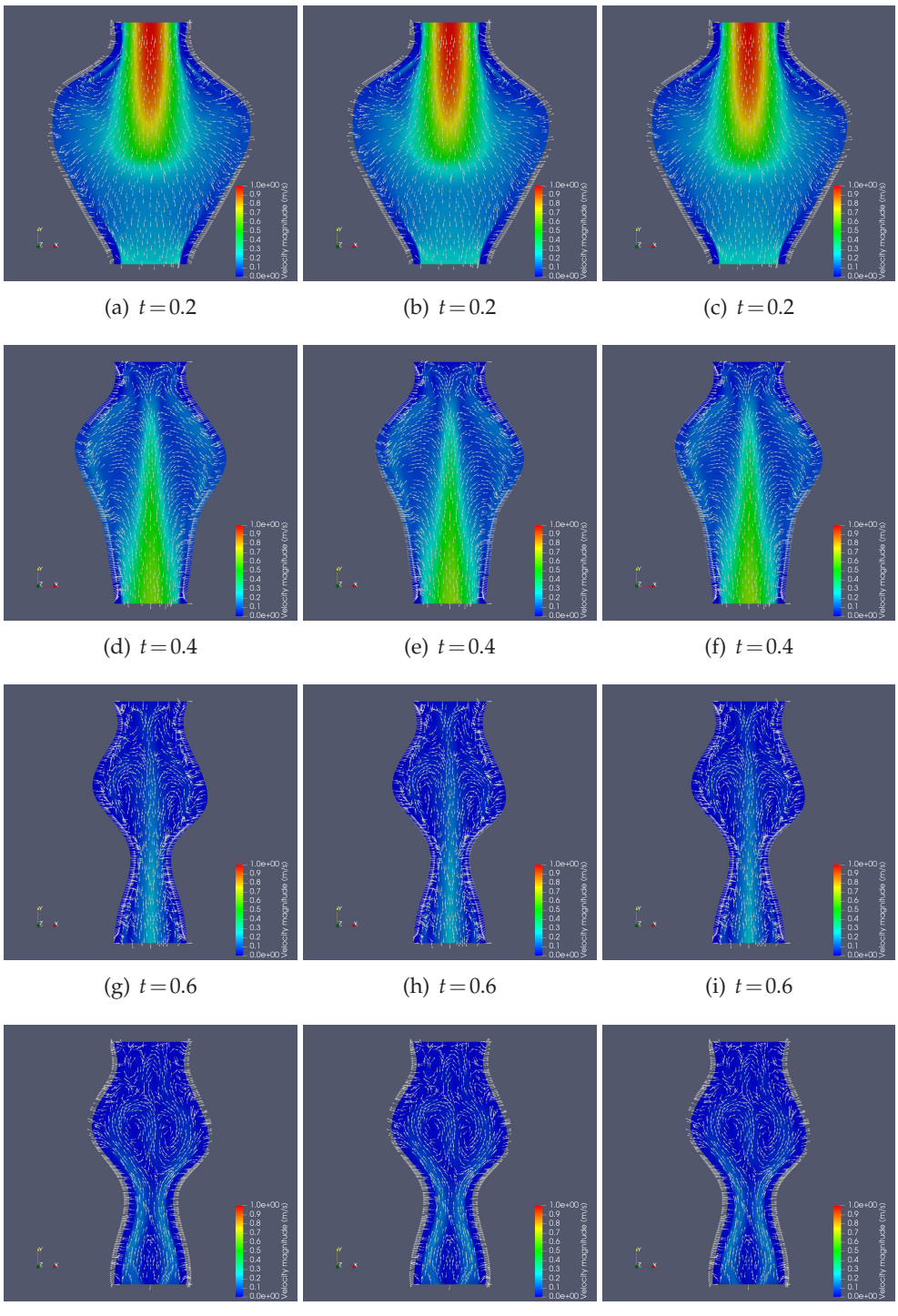

(a) $t=0.2$ (b) $t=0.2$ (c) $t=0.2$

(d) $t=0.4$ (e) $t=0.4$ (f) $t=0.4$

(g) $t=0.6$ (h) $t=0.6$ (i) $t=0.6$

(j) $t=0.8$ (k) $t=0.8$ (l) $t=0.8$

Figure 11: Velocity distributions at $t=0.2$, 0.4, 0.6, 0.8 s obtained by the coupled implicit scheme (left), the multirate β scheme with $r=1$ (middle) and $r=10$ (right) with fine mesh and $\Delta t_s = 0.0001$.

5 Concluding Remarks

Fluid structure interaction models appear in many engineering and science applications. As these models possess different time scales, it is natural to apply a multirate time-step strategy to solve them numerically. In this paper, we develop multirate β schemes for solving FSI problems with the added-mass effects. We validate the algorithms by testing a benchmark model involving a Stokes flow interacting a thin-walled structure and a general FSI model involving nonlinearity, irregular domains, and large structural deformations. It is notable that our algorithms are decoupled and added-mass free. Compared with the coupled implicit scheme, our algorithm uses much less computational cost to achieve the same order of accuracy.

6 Acknowledgement

The first and the third authors' research is supported in part by the Hong Kong RGC Competitive Earmarked Research Grant HKUST16301218 and NSFC (91530319,11772281). The second author's work is supported in part by the NIH BUILD grant (ASCEND pilot project) through UL1GM118973, the NSF HBCU-UP Research Initiation Award through HRD-1700328 and the NSF HBCU-UP Excellence in Research Award through DMS-1831950.

References

[1] S. Badia, F. Nobile, C. Vergara, Fluid–structure partitioned procedures based on Robin transmission conditions, J. Comput. Phys. 227 (14) (2008) 7027–7051.

[2] S. Badia, F. Nobile, C. Vergara, Robin–Robin preconditioned krylov methods for fluid–structure interaction problems, Comput. Methods Appl. Mech. Eng. 198 (33-36) (2009) 2768–2784.

[3] S. Badia, A. Quaini, A. Quarteroni, Splitting methods based on algebraic factorization for fluid-structure interaction, SIAM J. Sci. Comput.30 (4) (2008) 1778–1805.

[4] Y. Bazilevs, V. M. Calo, Y. Zhang, T. J. Hughes, Isogeometric fluid–structure interaction analysis with applications to arterial blood flow, Comput. Mech. 38 (4-5) (2006) 310–322.

[5] Y. Bazilevs, M.-C. Hsu, J. Kiendl, R. Wüchner, K.-U. Bletzinger, 3D simulation of wind turbine rotors at full scale. part ii: Fluid–structure interaction modeling with composite blades, Int. J. Numer. Methods Fluids 65 (1-3) (2011) 236–253.

[6] M. Bukac, B. Muha, Stability and convergence analysis of the extensions of the kinematically coupled scheme for the fluid-structure interaction, SIAM J. Numer. Anal. 54 (5) (2016) 3032–3061.

[7] H.-J. Bungartz, M. Schäfer, Fluid-structure interaction: modelling, simulation, optimisation, vol. 53, Springer Science & Business Media, 2006.

[8] M. Cai, M. Mu, and J. Xu, Numerical solution to a mixed Navier-Stokes/Darcy model by the two-grid approach. SIAM J. Numer. Anal. 47(5) (2009) 3325-3338.

[9] M. Cai, P. Huang, and M. Mu, Some multilevel decoupled algorithms for a mixed Navier-Stokes/Darcy model. Adv. Comput. Math., 44(1), (2018) pp.115-145.

[10] P. Causin, J.-F. Gerbeau, F. Nobile, Added-mass effect in the design of partitioned algorithms for fluid–structure problems, Comput. Methods Appl. Mech. Eng., 194 (42-44) (2005) 4506–4527.

[11] M. A. Fernández, J. Mullaert, M. Vidrascu, Explicit Robin–Neumann schemes for the coupling of incompressible fluids with thin-walled structures, Comput. Methods Appl. Mech. Eng., 267 (2013) 566–593.

[12] C. Förster, W. A. Wall, E. Ramm, Artificial added mass instabilities in sequential staggered coupling of nonlinear structures and incompressible viscous flows, Comput. Methods Appl. Mech. Eng., 196 (7) (2007) 1278–1293.

[13] L. Gerardo-Giorda, F. Nobile, C. Vergara, Analysis and optimization of Robin–Robin partitioned procedures in fluid-structure interaction problems, SIAM J. Numer. Anal. 48 (6) (2010) 2091–2116.

[14] W. Hao, S. Gong, S. Wu, J. Xu, M. R. Go, A. Friedman, and D. Zhu, A mathematical model of aortic aneurysm formation. PloS one 12.2 (2017): e0170807.

[15] T. He, A CBS-based partitioned semi-implicit coupling algorithm for fluidstructure interaction using MCIBC method. Comput. Methods Appl. Mech. Eng. 298 (2016): 252-278.

[16] T. He, K. Zhang, and T. Wang, AC-CBS-based partitioned semi-implicit coupling algorithm for fluid-structure interaction using stabilized second-order pressure scheme. Commun. Comput. Phys. 21.5 (2017): 1449-1474.

[17] U. Küttler, W. A. Wall, Fixed-point fluid–structure interaction solvers with dynamic relaxation, Comput. Mech. 43 (1) (2008) 61–72.

[18] M. Mu and J. Xu, A two-grid method of a mixed Stokes/Darcy model for coupling fluid flow with porous media flow. SIAM J. Numer. Anal., 45(5), (2007) pp.1801-1813.

[19] M. Mu and X. Zhu, Decoupled schemes for a non-stationary mixed Stokes-Darcy model, Math. Comput., 79(270), (2010) 707-731.

[20] F. Nobile, C. Vergara, An effective fluid-structure interaction formulation for vascular dy-

namics by generalized Robin conditions, SIAM J. Sci. Comput. 30 (2) (2008) 731–763.
[21] I. Rybak, J. Magiera, A multiple-time-step technique for coupled free flow and porous medium systems, J. Comput. Phys. 272 (2014) 327–342.
[22] L. Shan, H. Zheng, W. J. Layton, A decoupling method with different subdomain time steps for the nonstationary Stokes–Darcy model, Numerical Methods for Partial Differential Equations 29 (2) (2013) 549–583.
[23] A. Prakash,and K. D. Hjelmstad, A FETI based multi time step coupling method for Newmark schemes in structural dynamics. Int. J. Numer. Methods. Eng. 61.13 (2004): 2183-2204.
[24] A. Prakash, E. Taciroglu, and K. D. Hjelmstad, Computationally efficient multi-time-step method for partitioned time integration of highly nonlinear structural dynamics. Comput. Struct. 133 (2014): 51-63.
[25] A. Timalsina, G. Hou, and J. Wang, Computing fluid-structure interaction by the partitioned approach with direct forcing. Commun. Comput. Phys. 21.1 (2017): 182-210.
[26] R. Torii, M. Oshima, T. Kobayashi, K. Takagi, T. E. Tezduyar, Fluid–structure interaction modeling of aneurysmal conditions with high and normal blood pressures, Comput. Mech. 38 (4-5) (2006) 482–490.
[27] S. Turek, J. Hron, Proposal for numerical benchmarking of fluid-structure interaction between an elastic object and laminar incompressible flow, in: Fluid-structure interaction, Springer, 2006, pp. 371–385.
[28] T. Tezduyar and S. Sathe, Stabilization parameters in SUPG and PSPG formulations, Journal of computational and applied mechanics 4.1 (2003): 71-88.
[29] T. Wick, Solving monolithic fluid-structure interaction problems in arbitrary Lagrangian Eulerian coordinates with the deal. ii library.